# Phase competition in trisected superconducting dome

I. M. Vishik[a,b], M. Hashimoto[c], Rui-Hua He[d], Wei-Sheng Lee[a,b], Felix Schmitt[a,b], Donghui Lu[c], R. G. Moore[a], C. Zhang[e], W. Meevasana[f], T. Sasagawa[g], S. Uchida[h], Kazuhiro Fujita[i], S. Ishida[h], M. Ishikado[j], Yoshiyuki Yoshida[k], Hiroshi Eisaki[k], Zahid Hussain[l], Thomas P. Devereaux[a,b], and Zhi-Xun Shen[a,b,1]

[a]Stanford Institute for Materials and Energy Sciences and [c]Stanford Synchrotron Radiation Lightsource, SLAC National Accelerator Laboratory, Menlo Park, CA, 94025; [b]Geballe Laboratory for Advanced Materials, Departments of Physics and Applied Physics, Stanford University, Stanford, CA 94305; [d]Department of Physics, Boston College, Chestnut Hill, MA 02467; [e]State Key Laboratory of Crystal Materials, Shandong University, Jinan 250100, People's Republic of China; [f]School of Physics, Suranaree University of Technology, Muang, Nakhon Ratchasima 30000, Thailand; [g]Materials and Structures Laboratory, Tokyo Institute of Technology, Meguro-ku, Tokyo 152-8550, Japan; [h]Department of Physics, Graduate School of Science, University of Tokyo, Bunkyo-ku, Tokyo 113-0033, Japan; [i]Laboratory for Atomic and Solid State Physics, Department of Physics, Cornell University, Ithaca, NY 14853; [j]Quantum Beam Science Directorate, Japan Atomic Energy Agency, Tokai, Ibaraki 319-1195, Japan; [k]Superconducting Electronics Group, Electronics and Photonics Research Institute, National Institute of Advanced Industrial Science and Technology, Ibaraki 305-8568, Japan; and [l]Advanced Light Source, Lawrence Berkeley National Laboratory, Berkeley, CA 94720

Edited* by Elihu Abrahams, University of California, Los Angeles, CA, and approved September 27, 2012 (received for review June 4, 2012)

**A detailed phenomenology of low energy excitations is a crucial starting point for microscopic understanding of complex materials, such as the cuprate high-temperature superconductors. Because of its unique momentum-space discrimination, angle-resolved photoemission spectroscopy (ARPES) is ideally suited for this task in the cuprates, where emergent phases, particularly superconductivity and the pseudogap, have anisotropic gap structure in momentum space. We present a comprehensive doping- and temperature-dependence ARPES study of spectral gaps in $Bi_2Sr_2CaCu_2O_{8+\delta}$, covering much of the superconducting portion of the phase diagram. In the ground state, abrupt changes in near-nodal gap phenomenology give spectroscopic evidence for two potential quantum critical points, $p = 0.19$ for the pseudogap phase and $p = 0.076$ for another competing phase. Temperature dependence reveals that the pseudogap is not static below $T_c$ and exists $p > 0.19$ at higher temperatures. Our data imply a revised phase diagram that reconciles conflicting reports about the endpoint of the pseudogap in the literature, incorporates phase competition between the superconducting gap and pseudogap, and highlights distinct physics at the edge of the superconducting dome.**

quantum materials | correlated electrons | laser ARPES

The momentum-resolved nature of angle-resolved photoemission spectroscopy (ARPES) makes it a key probe of the cuprates, the interesting phases of which have anisotropic momentum-space structure (1–4): both the *d*-wave superconducting gap and the pseudogap above $T_c$ have a maximum at the antinode [AN, near (π, 0)] and are ungapped at the node, although the latter phase also exhibits an extended ungapped arc (5–8). Ordering phenomena often result in gapping of the quasiparticle spectrum, and distinct quantum states produce spectral gaps with characteristic temperature, doping, and momentum dependence. These phenomena were demonstrated by recent ARPES experiments that argued that the pseudogap is a distinct phase from superconductivity based on their unique phenomenology (8–15): the pseudogap dominates near the AN (8, 11), and its magnitude increases with underdoping (11, 12), whereas near-nodal (NN) gaps have a different doping dependence and can be attributed to superconductivity because they close at $T_c$ (8, 12). Previous measurements focused on AN or intermediate (IM) momenta, but laser-ARPES, with its superior resolution and enhanced statistics, allows for precise gap measurements near the node where the gap is smallest. Our work is unique in its attention to NN momenta using laser-ARPES, and we demonstrate, via a single technique, that three distinct quantum phases manifest in different NN phenomenology as a function of doping.

## Results

Gaps at parallel cuts were determined by fitting symmetrized energy distribution curves (EDCs) at $k_F$ to a minimal model (16). The Fermi wavevector, $k_F$, is defined by the minimum gap locus. Example spectra, raw and symmetrized EDCs at $k_F$, and fits are shown for UD92 (underdoped, $T_c = 92$) in Fig. 1.

**Low Temperature.** Fig. 2 *A–C* shows gaps around the Fermi surface (FS) in terms of the simple *d*-wave form, $0.5|\cos(k_x) - \cos(k_y)|$, measured $T \sim 10$K for the samples in our study (see *SI Appendix* for more details). These data are quantified by the gap slope, $v_\Delta$, which measures how fast the *d*-wave gap increases as a function of momentum away from the node. We find that the low-temperature $v_\Delta$ changes suddenly at two dopings, $p = 0.076$ and $p = 0.19$, which are marked in the energy-doping phase diagram in Fig. 2*D*, dividing the superconducting dome into three regions, labeled A, B, and C. In a *d*-wave superconductor, $v_\Delta$ is expected to scale with $T_c$, and in region C ($p > 0.19$) (Fig. 2*C*), $v_\Delta$ and $T_c$ indeed decrease together. Region B ($0.076 \leq p \leq 0.19$), exhibits a markedly different behavior: NN gaps are almost coincident over a large portion of the FS for all samples shown in Fig. 2*B*, indicating a doping-independent $v_\Delta$, despite $T_c$ varying more than twofold. The laser-ARPES gap functions show a slight curvature, nearly identical for all dopings, which is not visible in synchrotron-ARPES data because of poorer resolution and a sparser sampling of momenta. We note that the crossover between regions B and C is very abrupt, as $v_\Delta$ decreases by almost 25% for a change in doping $\Delta p = 0.01$, after having been constant within error bars for $\Delta p = 0.12$. There is also a very abrupt transition between regions A and B at $p = 0.076$ (Fig. 2*A*), as region A is marked by a FS which is gapped at every momentum. The gap minimum ($\Delta_{node}$) is at the nodal momentum [along (0, 0) − (π, π)] and increases with underdoping. Although $v_\Delta$ is no longer defined, the gap is still anisotropic around the FS. We define a gap anisotropy parameter in region A, $v_A$, from the momentum dependence of the gap in Fig. 2*A*, and $v_A$ decreases with underdoping. The low-temperature NN energy scales that characterize each of the three phase regions are summarized in Fig. 2*D*. These findings are an important refinement to previous results, which indicated that the NN region is dominated by superconductivity. These results demonstrate more conventional *d*-wave superconductivity in region C, unconventional doping-independent *d*-wave superconductivity in

Author contributions: R.-H.H., Z.H., T.P.D., and Z.-X.S. designed research; I.M.V., M.H., W.-S.L., F.S., D.L., R.G.M., C.Z., W.M., T.S., S.U., K.F., S.I., M.I., Y.Y., and H.E. performed research; I.M.V. analyzed data; and I.M.V. wrote the paper.

The authors declare no conflict of interest.

*This Direct Submission article had a prearranged editor.

[1]To whom correspondence should be addressed. E-mail: zxshen@stanford.edu.

This article contains supporting information online at www.pnas.org/lookup/suppl/doi:10.1073/pnas.1209471109/-/DCSupplemental.

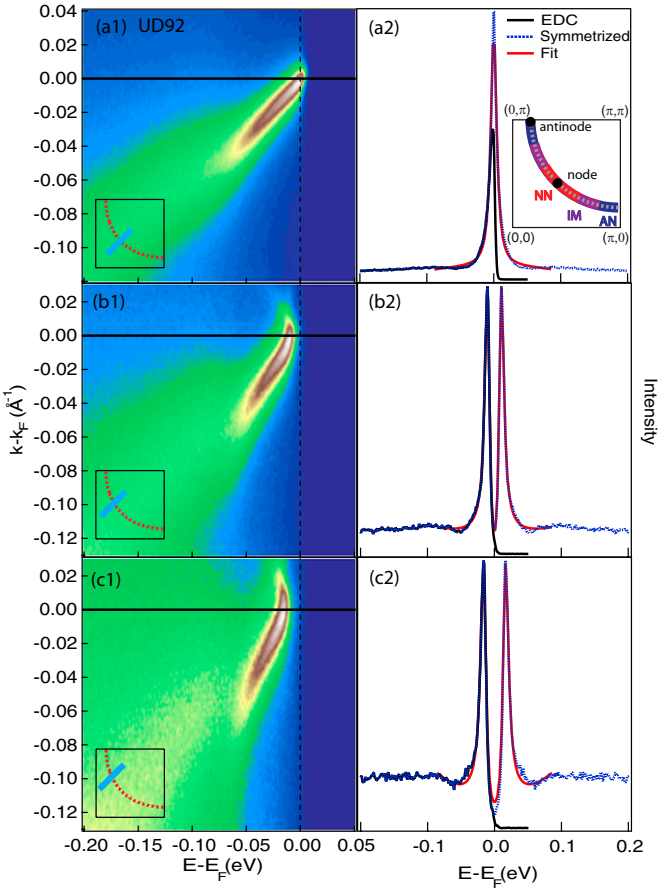


**Fig. 1.** Raw data, EDCs, and fitting. (*A1*, *B1*, *C1*) Spectra for UD92 at the node (*A1*) and away from the node (*B1* and *C1*), with cut geometry and position shown in insets. Horizontal lines are $k_F$. (*A2*, *B2*, *C2*) Raw (black) and symmetrized (blue) EDCs at $k_F$. EDCs are fit to a minimal model (16) (red) to extract gap. (*A2*, *Inset*) A quarter of the cuprate Brillouin zone and the FS (dotted line). The node and antinode points are identified with black dots. Locations of NN (red), IM (purple), and AN (blue) momenta are shown.

region B, and a nodeless unconventional superconductivity in region A.

**Temperature Dependence.** In Fig. 3 we compare low-temperature gaps with gaps just above $T_c$ in each of the three phase regions. For samples that are in region **A** at low temperature, the NN gaps are temperature-independent across $T_c$, and the FS remains fully gapped above $T_c$. This finding indicates that the gap at the nodal momentum does not have a purely superconducting origin and that the onset doping for region A is the same at low temperature and $T_c$. In region B, gaps close or diminish near the node at $T_c$ but AN gaps remain above $T_c$. This observation of Fermi arcs near the node, defined as momenta where the symmetrized EDCs at $k_F$ are peaked at $E_F$ (7), and gaps near the antinode are the usual ARPES signature of the pseudogap above $T_c$. All of the samples that exhibit characteristic doping-independent NN gaps of region B at low temperature also display a Fermi arc and antinodal gap above $T_c$. Additionally, OD80 ($p$~0.205) has an AN gap persisting $T>T_c$, demonstrating a pseudogap above $T_c$ at this doping. Thus, we classify the temperature dependence of OD80 with region B in Fig. 3 even though it exhibits region C phenomenology at low temperature. This finding suggests that the doping separating regions B and C may be different at low temperature and at $T_c$ and that the pseudogap may exist at higher temperature for $p > 0.19$. The most overdoped sample in our study, OD65, is the only one to exhibit an ungapped FS $T>T_c$, demonstrating that the normal state pseudogap persists until $p$~0.22, in agreement with other recent ARPES results (17).

We study temperature-and-doping dependence of gaps in two ways: doping dependence at comparable temperature and temperature dependence at varied dopings. The former is shown in Fig. 4 *A–C*, where three dopings (UD40, UD65, and UD92) are compared at three temperatures. These dopings are chosen to be in a regime where the superconductivity and pseudogap energy scales are well separated in Bi-2212 (*SI Appendix*). Two distinct doping dependencies are observed in different regions of the FS: doping-independent gaps and gaps which increase with underdoping. At 10K, doping-independent gaps are observed at NN and IM momenta, and gaps that increase with underdoping are observed at the AN. Just below $T_c$, however, doping-dependent gaps extend into the IM region. Above $T_c$, gaps increase with underdoping everywhere except the Fermi arc. Notably, a region of the FS (marked with a dashed box in Fig. 4 *A–C*) is home to doping-independent gaps at low temperatures but doping-dependent gaps near or above $T_c$. Fig. 4 *D* and *E* shows a full temperature dependence of gaps from low temperature to $T_c$ for UD55 and UD92. Temperature dependence near the node occurs in a limited temperature range within 25% of $T_c$, and the momentum region where gaps decrease near $T_c$ becomes larger with increasing doping.

## Discussion

**Phase Region A.** Whereas some ARPES experiments suggest a smooth evolution of phenomenology from the moderately underdoped regime to the edge of the superconducting dome (7, 18, 19), our data indicate an emergent phase in region A ($p <$ 0.076) that coexists with superconductivity, characterized in ARPES by a gap at every FS momentum. These results are supported by similar data in other cuprates. A fully gapped state at the underdoped edge of the superconducting dome has been shown in $Ca_{2-x}Na_xCuO_2Cl_2$ (Na-CCOC) (20) and $Bi_2Sr_{2-x}La_xCuO_{6+\delta}$ (La-Bi2201) (21), and our study demonstrates a fully gapped FS, both above and below $T_c$, in Bi-2212 at superconducting dopings. It is possible that region A represents an extension of pseudogap physics, but multiple spectroscopic changes $p < 0.076$ together with reports of a distinct order at the underdoped edge of the superconducting dome in other compounds points to distinct physics. There are three abrupt changes in NN gap phenomenology at $p = 0.076$: a fully gapped FS appears, the gap anisotropy away from the nodal momentum starts to decrease, and the NN gaps become temperature-independent across $T_c$, such that Fermi arcs are not observed. The latter result connects to in-plane transport in deeply underdoped cuprates, which shows negative $d\rho_{ab}/dT$ before the superconducting transition (22). Notably, EDCs in region A remain sufficiently sharp near the nodal momentum (*SI Appendix*), such that it is unlikely that this behavior is primarily disorder driven. There have been recent reports of a similar critical doping $p$~0.07–0.10 in $YBa_2Cu_3O_y$ (YBCO), varyingly attributed to a metal-insulator quantum critical point (23), a Lifshitz transition (24), or spin density wave order (SDW) (25). Although a similar onset doping might suggest a common origin of phenomena observed in YBCO and Bi-2212, there are some inconsistencies—such as thermal conductivity data—that do not support a fully gapped FS at low dopings in YBCO (26). This discrepancy may be materials-dependent, reflecting differences in disorder and Fermiology. Alternately, the ground state in region A may exhibit intrinsic time or spatial variation such that different techniques are sensitive to different aspects, which is supported by neutron scattering and muon spin-relaxation measurements in YBCO, indicating slowly fluctuating spin order at the edge of the superconducting dome (27). It has

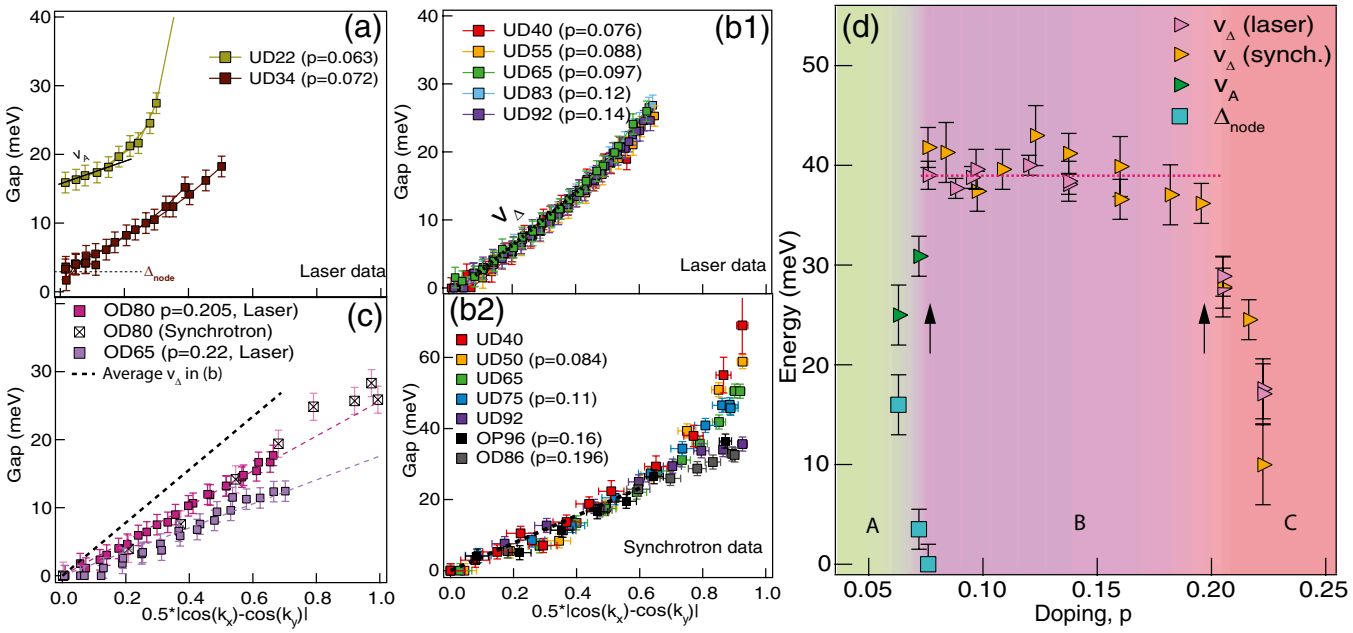


**Fig. 2.** Three distinct phase regions at low temperature. Label UD/OP/OD denotes underdoped/optimal/overdoped sample with $T_c$ given by the number which follows. Gaps plotted in terms of the simple *d*-wave form. $v_\Delta$ ($v_A$) is from a fit over the linear portion of the gap function, as shown by a solid or dotted line in *A* or *B1*, respectively. (*A*) In region A, FS is fully gapped with gap minimum, $\Delta_{node}$, at nodal momentum. Gap anisotropy $v_A$ decreases with underdoping. (*B*) Region B has doping-independent $v_\Delta$. (*C*) In region C, $v_\Delta$ decreases as $T_c$ decreases. Dashed line is guide-to-the-eye for average $v_\Delta$ observed in region B. Error bars in laser-ARPES reflect 3σ error in fitting procedure and an additional 100% margin. Error bars in synchrotron data reflect uncertainty of determining $E_F$ (±0.5 meV), error from fitting procedure, and an additional 100% margin. (*D*) Summary of low-temperature NN energy scales. Arrows mark critical dopings defining three phase regions.

been shown that SDW order can gap nodal quasiparticles (28), so this may be common to both compounds.

**Phase Regions B and C.** Although superconductivity has been shown to dominate at NN momenta (8, 9), Fig. 2*B* indicates that NN gaps are remarkably insensitive to $T_c$ in a broad doping range constituting region B, highlighting that NN gaps in region B do not reflect the bare superconducting order parameter. This doping-independent $v_\Delta$ is supported by specific heat measurements in YBCO (29) and from scanning tunneling spectroscopy (STS) data in Bi-based cuprates (30, 31). Our data are the most complete ARPES demonstration of this behavior, crucially revealing $p$ =

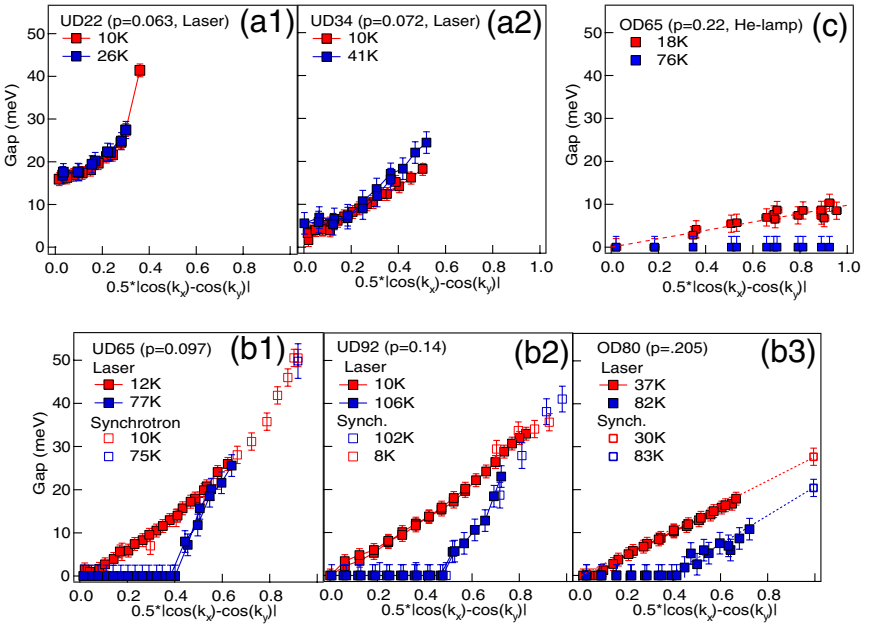


**Fig. 3.** Distinct temperature dependence of gap in each of three phase regions. Red: low temperature gap. Blue: gap $T>T_c$. (*A*) In region A, NN gaps do not close across $T_c$. (*B*) In region B, NN gaps partially close at $T_c$, with AN pseudogap remaining $T>T_c$. OD80 is in phase region C at low temperature, but behaves like phase region B $T>T_c$. (*C*) He-lamp data. For $p \geq 0.22$, gap closes everywhere on FS $T>T_c$.

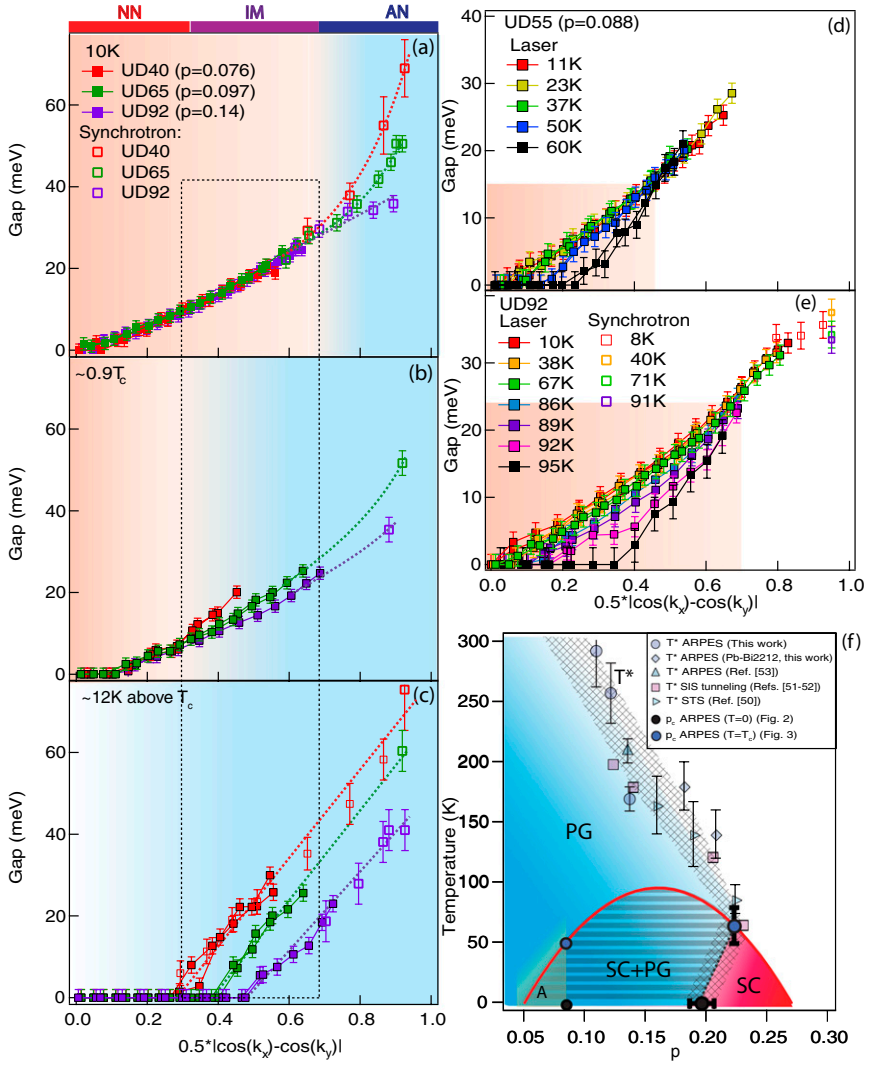


**Fig. 4.** Phase competition in region B (*A*–*C*) Gaps in UD40, UD65, and UD92 at 10K, 0.9 $T_c$, and 12 K above $T_c$. Synchrotron and laser data shown with open and filled symbols, respectively. Dashed lines are guides to the eye. Doping-independent or dependent gaps indicated by pink or blue shading, respectively. Dashed box marks momenta where gaps are doping-dependent in *B* and *C* but doping-independent in *A*. (*D* and *E*) Gap functions at various temperatures below and across $T_c$ for UD55 and UD92 (see *SI Appendix* for additional dopings). Shaded regions denotes momenta where the gap $T>T_c$ is smaller than the low temperature gap. Filled and open symbols are laser and synchrotron-ARPES data, respectively. (*F*) Proposed phase diagram. *T** is determined from ARPES measurements at antinode (*SI Appendix* and ref. 53), STS (50), and superconductor-insulator-superconductor tunneling (51, 52).

0.076 and $p = 0.19$ as dopings where region B abruptly ends. The sudden change in $v_\Delta$ at $p = 0.19$ is interpreted as the $T = 0$ endpoint of the pseudogap. This assignment has a precedent from low-temperature experiments, which indicated that both the superfluid density and the Cu-site impurity-doping needed to suppress superconductivity are maximum at $p = 0.19$ (29, 32, 33). Additionally, earlier ARPES data showed a maximum in the antinodal quasiparticle spectral weight, one measure of the strength of superconductivity relative to other spectral features, at $p = 0.19$ (34). In the interpretation that $p = 0.19$ is the $T = 0$ endpoint of the pseudogap, the more conventional relation between $T_c$ and $v_\Delta$ in region C reflects a pure superconducting ground state at low temperature, and region B is identified as a coexistence regime of superconductivity and the pseudogap. Coexistence of superconductivity and pseudogap in region B has support both from other experiments and from independent ARPES data in our study. STS experiments show symmetry-breaking order associated with the pseudogap throughout this doping range (35), and intrinsic tunneling spectroscopy shows distinct superconducting and pseudogap features below $T_c$ (36). In the present study, for all of region B, coexistence of pseudogap and superconductivity in Bi-2212 manifests via distinct temperature dependence of gaps near the node and further away from the node (8). For the most underdoped portion of region B ($p < 0.12$), coexistence also manifests in a gap function that deviates strongly from a simple *d*-wave form at the AN, such that $v_\Delta < \Delta_{AN}$, where $\Delta_{AN}$ is the AN gap (*SI Appendix*). The doping where $\Delta_{AN}$ first surpasses $v_\Delta$ is not significant, and simply indicates the doping where the superconducting gap (NN) energy scale is sufficiently smaller than the pseudogap (AN) energy scale. For some lower $T_c$ cuprates, gaps already deviate from a simple *d*-wave form at optimal doping and show stronger deviation than Bi-2212 in the underdoped regime (9, 12, 37). Although the pseudogap is considered to be primarily an AN phenomenon, our results demonstrate that it also manifests at NN momenta in region B via the doping-independent $v_\Delta$. Similarly, the absence of the pseudogap in the ground state $p > 0.19$ is also apparent at NN momenta, via a doping-dependent $v_\Delta$. The remarkable doping-independent $v_\Delta$ in region B remains unexplained, but it

may indicate a superconducting gap whose magnitude is renormalized by coexistence with the pseudogap.

The temperature dependence of spectral gaps provides microscopic information about the dynamics of the superconductivity/pseudogap coexistence in region B. Fig 4 *A–C* demonstrates that at IM momenta, gaps have characteristic doping dependence of $T^*$—increasing with underdoping (38, 39)—when superconductivity is weak just below $T_c$ or absent above $T_c$, but are doping-independent at low temperatures. This finding shows that the pseudogap is not static below $T_c$, but rather, it is suppressed by superconductivity at low temperatures. This nuance within the "two-gap" picture indicates that the temperature dependence of the pseudogap must also be considered for quantitative understanding of the superconducting state. Fig. 4 *A–C* shows that the Fermi arc just above $T_c$ does not represent the only momenta where superconductivity emerges, because the doping-independent gap region at $T$ = 10K extends beyond the Fermi arc measured $T>T_c$. A better way to define momenta with superconducting character is by temperature dependence near $T_c$, and the superconductivity-dominated momentum region defined in this manner expands with doping. Although a pure superconducting gap closes entirely at $T_c$, we use a more lenient definition—a gap which diminishes approaching $T_c$—to define momenta with superconducting character. We note that superconductivity exists over the entire FS in Bi-2212, as sharp quasiparticles are observed at the AN for $p > 0.08$ (34, 40, 41), but our definition of the "superconducting region" selects the portion of the FS where the temperature dependence of gaps indicates significant spectral contributions from superconductivity. This definition also permits for coexistence of pseudogap and superconductivity at some momenta, accounts for the observation that the pseudogap itself has temperature dependence, and is not hindered by difficulties in defining the Fermi arc length because of its temperature dependence (7). The temperature-dependence data in Fig. 4 *A–E* provides a phase-competition picture of superconductivity/pseudogap interaction in momentum space: the pseudogap is suppressed by superconductivity at low temperatures and larger dopings, and it surrenders a portion of the FS where it once existed.

**Proposed Phase Diagram.** The starting point of the phase diagram proposed in Fig. 4*F* is the observation of three distinct phase regions at low temperature as a function of doping, separated by two potential quantum critical points inside the superconducting dome at $p = 0.076$ and $p = 0.019$. The former marks the onset of region A, possibly related to SDW order, and the latter is interpreted as the $T = 0$ endpoint of the pseudogap. Both critical points have support from other experiments in numerous cuprates (20, 23, 25, 29, 32, 33, 42), and some theoretical proposals also favor a ground state with multiple critical points (43). Our data demonstrate how these potential critical points manifest in the phenomenology of NN spectral gaps measured by ARPES. The phase diagram in Fig. 4*F* also features conjectured reentrant behavior of the pseudogap inside the superconducting dome, as a direct consequence of phase competition between superconductivity and the pseudogap (44–46). The phase boundary between regions B (SC+PG) and C (SC) is anchored by ARPES data at $T = 0$ and $T = T_c$, which show a sudden change in $v_\Delta$ and an absence of pseudogap $T>T_c$, respectively. These data are supported by OD80, data which obey region C phenomenology at low temperature, but region B phenomenology at higher temperature, with the pseudogap persisting above $T_c$. It has been shown that the $T = 0$ endpoint of a competing order is expected to shift under the superconducting dome (47), such that high-temperature measurements of the pseudogap phase boundary do not extrapolate to the $T = 0$ endpoint seen inside the superconducting dome. This result manifests clearly in the $BaFe_2As_2$ family of iron pnictide compounds where both magnetic and structural phases have been shown to coexist with and be suppressed by superconductivity (48, 49), and a phase diagram with reentrant behavior has been demonstrated (49). A phase diagram with a reentrant pseudogap resolves conflicting reports about the fate of the pseudogap transition temperature, $T^*$, inside the superconducting dome. Some experiments suggest that the $T^*$ line intersects the superconducting dome and reaches $T = 0$ at $p = 0.19$ (29, 38), whereas others, particularly spectroscopies, including our ARPES measurements of $T^*$ shown in Fig. 4*F*, indicate that $T^*$ and $T_c$ merge on the strongly overdoped side (17, 50–53). Although variations between different experiments are expected, our data uniquely demonstrate both behaviors using a single technique.

## Conclusions

We have performed a thorough doping-and-temperature dependence study of spectral gaps in superconducting Bi-2212. At low temperature, we report three distinct phase regions with different characteristic phenomenology of NN gaps. In phase region B ($0.076 < p < 0.19$), which is identified as a regime where superconductivity coexists with the pseudogap in the ground state, gaps at NN and IM momenta are independent of doping. In region C ($p > 0.19$), identified as a pure superconducting ground state, the *d*-wave superconducting gap decreases as $T_c$ decreases. Region A ($p < 0.076$) is identified as an emergent phase characterized by a fully gapped FS and a gap anisotropy that decreases with underdoping. Temperature dependence of gaps reveals phase competition between the pseudogap and superconductivity, where pseudogap physics dominate a smaller region of the FS at low temperatures and larger dopings. From these doping- and temperature-dependence data we propose a unique phase diagram featuring a trisected superconducting dome and reentrant behavior of the pseudogap.

## Materials and Methods

Laboratory-based experiments were done with 7 eV laser or monochromated He-I light (21.2 eV) (Gammadata He lamp) and a Scienta SES2002 analyzer. The 7 eV photons were produced by second harmonic generation from a 355-nm laser (Paladin; Coherent) using a nonlinear crystal $KBe_2BO_3F_2$. Laser energy and momentum resolution were 3 meV and better than 0.005 $Å^{-1}$, respectively. Synchrotron data were taken at the Stanford Synchrotron Radiation Lightsource with a Scienta R4000 analyzer and energy resolution ~8 meV. Samples were cleaved at 10–30K in situ at a pressure $<4 \times 10^{-11}$ torr to obtain a clean surface. Doping was determined from $T_c$ via an empirical curve, $T_c = T_{c,max}*[1-82.6(p - 0.16)^2]$, taking 96K as the optimum $T_c$ for Bi-2212 (54).

During the review process, following the submission of this manuscript, related papers appeared in support of charge density wave order, possibly related to the pseudogap, which competes with superconductivity (55, 56). In addition, another paper reported a gap at the nodal momentum in $La_{2-x}Sr_xCuO_4$ (57).

**ACKNOWLEDGMENTS.** This work is supported by the Department of Energy, Office of Basic Energy Science, Division of Materials Science. Work at SSRL is supported by the office's Division of Scientific User Facilities.

1. Shen Z-X, et al. (1993) Anomalously large gap anisotropy in the *a-b* plane of $Bi_2Sr_2CaCu_2O_{8+\delta}$. *Phys Rev Lett* 70(10):1553–1556.
2. Loeser AG, et al. (1996) Excitation gap in the normal state of underdoped $Bi_2Sr_2CaCu_2O_{8+\delta}$. *Science* 273(5273):325–329.
3. Ding H, et al. (1996) Angle-resolved photoemission spectroscopy study of the superconducting gap anisotropy in Bi2Sr2CaCu2O8+x. *Phys Rev B Condens Matter* 54(14): R9678–R9681.
4. Ding H, et al. (1996) Spectroscopic evidence for a pseudogap in the normal state of underdoped high-$T_c$ superconductors. *Nature* 382:51–54.
5. Marshall DS, et al. (1996) Unconventional electronic structure evolution with hole doping in $Bi_2Sr_2CaCu_2O_{8+\delta}$: Angle-resolved photoemission results. *Phys Rev Lett* 76 (25):4841–4844.
6. Norman MR, et al. (1998) Destruction of the Fermi surface in underdoped high-$T_c$ superconductors. *Nature* 392:157–160.

7. Kanigel A, et al. (2006) Evolution of the pseudogap from Fermi arcs to the nodal liquid. *Nat Phys* 2:447–451.
8. Lee WS, et al. (2007) Abrupt onset of a second energy gap at the superconducting transition of underdoped Bi2212. *Nature* 450(7166):81–84.
9. Kondo T, Khasanov R, Takeuchi T, Schmalian J, Kaminski A (2009) Competition between the pseudogap and superconductivity in the high-*T*(c) copper oxides. *Nature* 457(7227):296–300.
10. Hashimoto M, et al. (2010) Particlehole symmetry breaking in the pseudogap state of Bi2201. *Nat Phys* 6:414–417.
11. Tanaka K, et al. (2006) Distinct Fermi-momentum-dependent energy gaps in deeply underdoped Bi2212. *Science* 314(5807):1910–1913.
12. Yoshida T, et al. (2009) Universal versus material-dependent two-gap behaviors of the high-$T_c$ cuprate superconductors: Angle-resolved photoemission study of $La_{2-x}Sr_xCuO_4$. *Phys Rev Lett* 103(3):037004.
13. Kondo T, Takeuchi T, Kaminski A, Tsuda S, Shin S (2007) Evidence for two energy scales in the superconducting state of optimally doped $(Bi,Pb)_2(Sr,La)_2CuO_{6+\delta}$. *Phys Rev Lett* 98(26):267004.
14. He R-H, et al. (2011) From a single-band metal to a high-temperature superconductor via two thermal phase transitions. *Science* 331(6024):1579–1583.
15. Ma J-H, et al. (2008) Coexistence of competing orders with two energy gaps in real and momentum space in the high temperature superconductor Bi_2Sr_2-xLa_xCuO_6 +delta. *Phys Rev Lett* 101(20):207002.
16. Norman MR, Randeria M, Ding H, Campuzano JC (1998) Phenomenology of the low-energy spectral function in high-$T_c$ superconductors. *Phys Rev B* 57:R11093–R11096.
17. Chatterjee U, et al. (2011) Electronic phase diagram of high-temperature copper oxide superconductors. *Proc Natl Acad Sci USA* 108(23):9346–9349.
18. Chatterjee U, et al. (2010) Observation of a *d*-wave nodal liquid in highly underdoped $Bi_2Sr_2CaCu_2O_{8+\delta}$. *Nat Phys* 6:99–103.
19. Yang H-B, et al. (2011) Reconstructed Fermi surface of underdoped $Bi_2Sr_2CaCu_2O_{(8+\delta)}$ cuprate superconductors. *Phys Rev Lett* 107(4):047003.
20. Shen KM, et al. (2004) Fully gapped single-particle excitations in lightly doped cuprates. *Phys Rev B* 69(5):054503.
21. Hashimoto M, et al. (2008) Doping evolution of the electronic structure in the single-layer cuprate $Bi_2Sr_{2-x}La_xCuO_{6+\delta}$: Comparison with other single-layer cuprates. *Phys Rev B* 77(9):094516.
22. Ando Y, Komiya S, Segawa K, Ono S, Kurita Y (2004) Electronic phase diagram of high-$T_c$ cuprate superconductors from a mapping of the in-plane resistivity curvature. *Phys Rev Lett* 93(26 Pt 1):267001.
23. Sebastian SE, et al. (2010) Metal-insulator quantum critical point beneath the high $T_c$ superconducting dome. *Proc Natl Acad Sci USA* 107(14):6175–6179.
24. LeBoeuf D, et al. (2011) Lifshitz critical point in the cuprate superconductor *Y* $Ba_2Cu_3O_y$ from high-field Hall effect measurements. *Phys Rev B* 83:054506.
25. Haug D, et al. (2010) Neutron scattering study of the magnetic phase diagram of underdoped $YBa_2Cu_3O_{6+x}$. *New J Phys* 12:105006.
26. Sutherland M, et al. (2005) Delocalized fermions in underdoped cuprate superconductors. *Phys Rev Lett* 94(14):147004.
27. Hinkov V, et al. (2008) Electronic liquid crystal state in the high-temperature superconductor $YBa_2Cu_3O_{6.45}$. *Science* 319(5863):597–600.
28. Nazario Z, Santiago DI (2004) Coexistence of spin-density wave and *d*-wave superconducting order parameter. *Phys Rev B* 70(14):144513.
29. Tallon JL, Loram JW, Cooper JR, Panagopoulos C, Bernhard C (2003) Superfluid density in cuprate high-$T_c$ superconductors: A new paradigm. *Phys Rev B* 68(18): 180501.
30. Boyer MC, et al. (2007) Imaging the two gaps of the high-temperature superconductor $Bi_2Sr_2CuO_{6+x}$. *Nat Phys* 3:802–806.
31. Pushp A, et al. (2009) Extending universal nodal excitations optimizes superconductivity in $Bi_2Sr_2CaCu_2O_{8+\delta}$. *Science* 324(5935):1689–1693.
32. Anukool W, Barakat S, Panagopoulos C, Cooper JR (2009) Effect of hole doping on the London penetration depth in $Bi_{2.15}Sr_{1.85}CaCu_2O_{8+\delta}$ and $Bi_{2.1}Sr_{1.9}Ca_{0.85}Y_{0.15}Cu_2O_{8+\delta}$. *Phys Rev B* 80(2):024516.
33. Panagopoulos C, et al. (2003) Superfluid response in monolayer high-$T_c$ cuprates. *Phys Rev B* 67:220502.
34. Feng DL, et al. (2000) Signature of superfluid density in the single-particle excitation spectrum of Bi(2)Sr(2)CaCu(2)O(8+δ). *Science* 289(5477):277–281.
35. Parker CV, et al. (2010) Fluctuating stripes at the onset of the pseudogap in the high-*T* (c) superconductor Bi(2)Sr(2)CaCu(2)O(8+*x*). *Nature* 468(7324):677–680.
36. Krasnov VM, Yurgens A, Winkler D, Delsing P, Claeson T (2000) Evidence for coexistence of the superconducting gap and the pseudogap in Bi-2212 from intrinsic tunneling spectroscopy. *Phys Rev Lett* 84(25):5860–5863.
37. He R-H, et al. (2009) Energy gaps in the failed high-*T*c superconductor $La_{1.875}Ba_{0.125}CuO_4$. *Nat Phys* 5:119–123.
38. Tallon JL, Loram JW (2001) The doping dependence of *T** what is the real high-*T*c phase diagram? *Physica C* 349(1–2):53–38.
39. Campuzano JC, et al. (1999) Electronic spectra and their relation to the (pi, pi) collective mode in high-$T_c$ superconductors. *Phys Rev Lett* 83(18):3709.
40. Vishik IM, et al. (2009) A momentum-dependent perspective on quasiparticle interference in $Bi_2Sr_2CaCu_2O_{8+\delta}$. *Nat Phys* 5:718–721.
41. Niestemski LR, Wang Z (2009) Valence bond glass theory of electronic disorder and the pseudogap state of high-temperature cuprate superconductors. *Phys Rev Lett* 102 (10):107001.
42. Zheng G-Q, Kuhns PL, Reyes AP, Liang B, Lin CT (2005) Critical point and the nature of the pseudogap of single-layered copper-oxide $Bi_2Sr_{2-x}La_xCuO_{6+\delta}$ superconductors. *Phys Rev Lett* 94(4):047006.
43. Chakravarty S (2011) Quantum oscillations and key theoretical issues in high temperature superconductors from the perspective of density waves. *Rep Prog Phys* 74: 022501.
44. Wu J-B, Pei M-X, Wang Q-H (2005) Competing orders and interlayer tunneling in cuprate superconductors: A finite-temperature Landau theory. *Phys Rev B* 71(17): 172507.
45. Gabovich AM, et al. (2010) Competition of superconductivity and charge density waves in cuprates: Recent evidence and interpretation. *Adv Cond Mat Phys* 2010: 681070.
46. Ekino T, et al. (2011) The phase diagram for coexisting *d*-wave superconductivity and charge-density waves: Cuprates and beyond. *J Phys Condens Matter* 23(38):385701.
47. Moon EG, Sachdev S (2010) Quantum critical point shifts under superconductivity: Pnictides and cuprates. *Phys Rev B* 82(10):104516.
48. Wiesenmayer E, et al. (2011) Microscopic coexistence of superconductivity and magnetism in $Ba_{(1-x)}K_{(x)}Fe_2As_2$. *Phys Rev Lett* 107(23):237001.
49. Nandi S, et al. (2010) Anomalous suppression of the orthorhombic lattice distortion in superconducting $Ba(Fe_{1-x}Co_x)_2As_2$ single crystals. *Phys Rev Lett* 104(5):057006.
50. Gomes KK, et al. (2007) Visualizing pair formation on the atomic scale in the high-$T_c$ superconductor $Bi_2Sr_2CaCu_2O_{8+\delta}$. *Nature* 447(7144):569–572.
51. Dipasupil RM, Oda M, Momono N, Ido M (2002) Energy gap evolution in the tunneling spectra of $Bi_2Sr_2CaCu_2O_{8+\delta}$. *J Phys Soc Jpn* 71(6):1535–1540.
52. Ozyuzer L, Zasadzinski JF, Gray KE, Kendziora C, Miyakawa N (2002) Absence of pseudogap in heavily overdoped $Bi_2Sr_2CaCu_2O_{8+\delta}$ from tunneling spectroscopy of break junctions. *Europhys Lett* 58(4):589–595.
53. Kondo T, et al. (2011) Disentangling Cooper-pair formation above the transition temperature from the pseudogap state in the cuprates. *Nat Phys* 7:21–25.
54. Tallon JL, Bernhard C, Shaked H, Hitterman RL, Jorgensen JD (1995) Generic superconducting phase behavior in high-$T_c$ cuprates: $T_c$ variation with hole concentration in $YBa_2Cu_3O_{7-\delta}$. *Phys Rev B Condens Matter* 51(18):12911–12914.
55. Ghiringhelli G, et al. (2012) Long-range incommensurate charge fluctuations in (Y,Nd) $Ba_2Cu_3O_{6+x}$. *Science* 337(6096):821–825.
56. Chang J, et al. (2012) Direct observation of competition between superconductivity and charge density wave order in $YBa_2Cu_3O_y$. Available at http://arxiv.org/abs/1206.4333, accessed Aug. 10, 2012.
57. Razzoli E, et al. (2012) Evolution from a nodeless gap to $d(x^2-y^2)$ form in underdoped $La_{2-x}Sr_xCuO_4$. Available at http://arxiv.org/abs/1207.3486v1, accessed Aug. 10, 2012.